BIND-USBL: Bounding IMU Navigation Drift using USBL in Heterogeneous ASV–AUV Teams

Pranav Kedia[1,2], Rajini Makam[3], Heiko Hamann[1,2], and Suresh Sundaram[3]

***Abstract*—Accurate and continuous localization of Autonomous Underwater Vehicles (AUVs) in GPS-denied environments is a persistent challenge in marine robotics. In the absence of external position fixes, AUVs rely on inertial dead-reckoning, which accumulates unbounded drift due to sensor bias and noise. This paper presents BIND-USBL, a cooperative localization framework in which a fleet of Autonomous Surface Vessels (ASVs) equipped with Ultra-Short Baseline (USBL) acoustic positioning systems provides intermittent fixes to bound AUV dead-reckoning error. The key insight is that long-duration navigation failure is driven not by the accuracy of individual USBL measurements, but by the temporal sparsity and geometric availability of those fixes. BIND-USBL combines a multi-ASV formation model linking survey scale and anchor placement to acoustic coverage, a conflict-graph-based TDMA uplink scheduler for shared-channel servicing, and delayed fusion of received USBL updates with drift-prone dead reckoning. The framework is evaluated in the HoloOcean simulator using heterogeneous ASV-AUV teams executing lawnmower coverage missions. The results show that localization performance is shaped by the interaction of survey scale, acoustic coverage, team composition, and ASV-formation geometry. Further, The spatial-reuse scheduler improves per-AUV fix delivery rate without violating the no-collision constraint, while maintaining low end-to-end fix latency.**

***Index Terms*—AUV navigation, USBL acoustic positioning, IMU drift bounding, heterogeneous multi-robot systems, TDMA scheduling, ASV–AUV cooperation**

I. Introduction

Marine robotics is undergoing a transformative shift toward heterogeneous multi-vehicle systems in which *Autonomous Surface Vessels* (ASVs) and *Autonomous Underwater Vehicles* (AUVs) operate in coordinated teams to accomplish tasks that would be infeasible or prohibitively expensive with a single platform [1]. Applications include wide-area seafloor mapping, oceanographic sampling, search-and-rescue operations, infrastructure inspection, and persistent environmental monitoring [2]. In all such missions, accurate and continuous localization of the underwater agents is paramount: an AUV that does not know where it is cannot complete a survey, cannot rendezvous with a recovery vehicle, and cannot safely avoid hazards.

Ultra-Short Baseline (USBL) acoustic positioning is the most widely deployed solution for operational AUV localization. A USBL system uses a multi-element transducer array mounted on a surface vessel to exchange acoustic signals with an AUV-mounted transponder, estimating slant range via Two-Way Travel Time (TWTT) and bearing via Time Difference of Arrival (TDOA) [3]. By combining these measurements with the GNSS-referenced position of the surface vessel, an absolute AUV position fix is obtained. Compared to Long Baseline (LBL) systems, which require pre-deployed infrastructure, and surfacing-based localization, which disrupts missions, USBL provides a flexible and infrastructure-free alternative. USBL delivers frequent position updates over moderate ranges, thereby making it the de facto standard for ship-based AUV navigation support [4].

An alternative to the conventional USBL paradigm is *passive inverted USBL* (piUSBL), in which the hydrophone array is mounted on the AUV rather than the surface platform, and a single time-synchronized acoustic beacon broadcasts a known waveform at a fixed rate [5], [6]. Each AUV passively receives the signal and independently estimates its range via one-way travel time (OWTT) and bearing via onboard beamforming, eliminating the two-way interrogation cycle and enabling simultaneous localization of arbitrarily many vehicles from a single beacon [7]. Recent work has extended piUSBL to fully submerged multi-agent teams using bearing, elevation, and depth-difference (BEDD) measurements within a factor-graph framework, removing the requirement for a surface-expressed anchor entirely [8]. Open-source implementations such as Raspi2USBL [9] have further reduced the cost and accessibility barrier, demonstrating sub-decimetre ranging accuracy and bearing precision within 0.1° at ranges up to 1.3 km. While piUSBL offers compelling scalability for large fleets, it requires clock synchronization hardware (typically an oven-controlled crystal oscillator) on every vehicle and delegates all signal processing to the AUV, increasing onboard computational and power demands.

Replacing crewed support vessels with ASVs offers significant advantages in cost, safety, and operational autonomy. Autonomous wind-powered surface vessel (AWSV) teams [10] are emerging as particularly attractive platforms for this role, their energy autonomy removes the endurance constraints of battery- or fuel-driven ASVs, enabling persistent multi-day deployments as acoustic anchors without the need for recovery or refuelling [11], [12]. This makes AWSVs a natural candidate for the surface support layer envisioned by BIND-USBL, where sustained station-keeping at designated formation vertices is the primary operational requirement. Early work by Bremnes *et al.* [13] formalized this concept for single-AUV support, introducing a hybrid controller that maintains

[1]Dept of Computer and Information Science, University of Konstanz, Germany; [2]Centre for the Advanced Study of Collective Behaviour, University of Konstanz, Germany. {pranav.kedia, heiko.hamann}@uni-konstanz.de

[3]Dept of Aerospace Engineering, Indian Institute of Science, Bangalore, India. {rajinimakam, vssuresh}@iisc.ac.in

Corresponding author: Pranav Kedia

the ASV within a bounded operational region. This framework was extended to multi-AUV scenarios using a switching control architecture with Extended Kalman Filter (EKF) state estimation [14]. Complementary efforts demonstrated cooperative ASV–AUV systems with optimized acoustic protocols [4], and coordinated control strategies for search-and-rescue and trajectory tracking under communication constraints [15], [16].

Despite these advantages, USBL-based localization is constrained by azimuth estimation errors that grow proportionally with slant range [17], [18], systematic biases from installation misalignment [19], and acoustic propagation distortions from multipath and sound speed variations [4], [20]. In the intervals between USBL fixes, AUVs rely on IMU dead-reckoning, whose error grows unboundedly due to sensor noise, bias, and stochastic disturbances [21]. Practical cost-constrained deployments use low-cost MEMS IMUs that exhibit substantially higher drift rates than high-grade inertial systems, and whose uncertainties often exhibit non-Gaussian characteristics requiring robust estimation frameworks [22].

The accuracy of USBL localization is further influenced by the geometric relationship between the surface platform and the submerged vehicle, a dependency characterized via Fisher Information Matrix (FIM) analysis linking sensor geometry to Cramér–Rao bounds [23]. Active ASV repositioning to maximize information gain can significantly improve tracking accuracy [24]. Within the broader multi-AUV literature, cooperative strategies spanning formation control, coverage, and distributed estimation have been extensively studied [1], [25]–[28].

Despite these advances, a critical gap remains: how a *fleet* of ASVs can be systematically organized to provide bounded navigation support to multiple AUVs through coordinated scheduling and positioning. Existing works predominantly address single-ASV support for multiple AUVs [14] or analyze USBL measurement quality in isolation. The coupled interaction between scheduling policies, acoustic channel contention, fix availability, and AUV drift dynamics has not been rigorously treated.

This paper introduces BIND-USBL to address this gap. The key insight is that long-term navigation failure is driven not by the accuracy of individual USBL measurements, but by their *temporal sparsity*: as inter-fix intervals increase, dead-reckoning error grows unbounded. The objective of each ASV is to deliver localization updates with sufficient frequency and geometric diversity to bound the ensemble navigation error. The main contributions of BIND-USBL are:

(1) A multi-ASV formation geometry framework providing explicit acoustic coverage guarantees for the N-ASV, N-AUV setting via a corner-to-nearest-ASV bound and a closed-form minimum formation radius constraint.

(2) An acoustic conflict graph formulation and greedy graph-colouring scheduling policy that enables spatial reuse of the shared acoustic uplink channel while preventing inter-AUV interference.

(3) A TDMA slot-timing model whose guard intervals scale with the acoustic crossing time of the survey area, ensuring protocol validity across operational scales.

We also incorporate multi-ASV USBL fix fusion via an MVLUE formulation reduce fused-fix standard deviation by$1/\sqrt{K}$. The framework is validated in the HoloOcean [29] simulator with full vehicle dynamics, acoustic propagation delay, packet loss, and communication scheduling.

The remainder of this paper is organized as follows. Section II formulates the problem, presents vehicle dynamics, the USBL positioning model, multi-ASV geometry and scheduling, the IMU drift model, and the complementary filter fusion. Section III presents simulation results. Section IV concludes with findings and future directions.

II. BIND-USBL

A. Problem Formulation

Consider a multi-vehicle marine system comprising N_{AUV} AUVs and N_{ASV} ASVs operating in a square survey area $\Omega = [-L/2,\, L/2]^2 \subset \mathbb{R}^2$. GPS is unavailable underwater, so each AUV i propagates its position estimate via strapdown inertial dead-reckoning. Without external correction, this estimate diverges from the true position due to sensor bias $\mathbf{b}_i$ and process noise, with error growing unboundedly over time. Each ASV is equipped with a USBL transducer array and GNSS, enabling it to compute absolute position fixes for AUVs within acoustic range. ASV's primary task is to deliver drift-bounding position fixes.

The system operates a two-band acoustic architecture: a short-range high-frequency (HF) uplink channel on which AUVs ping requesting fixes, and a longer-range medium-frequency (MF) downlink channel on which ASVs broadcast the accumulated fix payload to AUVs. HF scheduling is managed by a TDMA protocol, whereas MF uses an event-triggered priority assignment.

The objective of BIND-USBL is to characterize how navigation accuracy depends on team composition and surface-formation geometry in heterogeneous ASV–AUV systems. For a given combination of AUVs and ASVs, the framework evaluates how the acoustic servicing rate, anchor placement, and multi-vehicle contention affect the achievable position error in practice. In this way, formation design is treated not as a mechanism for guaranteeing a prescribed bound, but as a system-level factor that shapes the trade-off between fix availability, localization quality, and resulting navigation accuracy.

B. Vehicle Dynamics

AUVs are modeled with 6-DOF nonlinear dynamics [2], [30]. In simulation, the navigation filter operates on the 2D horizontal position $\hat{\mathbf{p}}_i \in \mathbb{R}^2$; depth is handled independently via a pressure sensor.

The ASV is modeled as a 3-DOF surface craft (surge, sway, yaw) [30]. These dynamics are realized in HoloOcean [29]. A station-keeping controller holds the ASV near the survey centroid, $\mathbf{p}_{T,\mathrm{ASV}} \approx \mathrm{centroid}(\Omega)$, through continuous thruster operation while preserving favorable USBL geometry.

C. USBL Navigation Principle [31]

Each ASV estimates the relative position of an AUV using acoustic ranging and direction finding. The slant range is obtained from the round-trip travel time (RTT):

$$r = \frac{c\,\tau_{\mathrm{RTT}}}{2}, \tag{1}$$

where $c = 1500$ m/s is the nominal speed of sound.

The direction-of-arrival (DOA) is computed from the time-difference-of-arrival (TDOA) measurements across the five-element hydrophone array. The ASV calculates the absolute world-frame fix of each AUV by combining the GNSS position $\mathbf{p}_j^{\mathrm{ASV}}$ with the range $d_{ij} = c\,t_{\mathrm{RTT}}/2$ and the TDOA-derived direction angles (θ, ϕ) (azimuth, elevation):

$$\mathbf{z}_{ij,k} = \mathbf{p}_{j,k}^{\mathrm{ASV}} + d_{ij} \begin{bmatrix} \cos\phi\cos\theta \\ \cos\phi\sin\theta \\ \sin\phi \end{bmatrix} + \boldsymbol{\epsilon}_{\mathrm{USBL}}, \tag{2}$$

where, $i \in [1, N_{AUV}]$, $j \in [1, N_{ASV}]$, $\boldsymbol{\epsilon}_{\mathrm{USBL}} \sim \mathcal{N}(\mathbf{0}, \Sigma_{\mathrm{USBL}})$ encodes RTT quantisation, TDOA noise, and AHRS heading error. When more than one ASV simultaneously hears AUV i, the resulting multi-ASV fused fix is the minimum-variance linear unbiased estimator (MVLUE). This shows that deploying additional ASVs improves not only fix *availability* but also fix *quality*.

Acoustic fix loss due to attenuation, multipath, and channel contention is modelled probabilistically. The range-dependent loss probability follows [31]:

$$P_{\mathrm{loss}}(r) = a\,e^{b\,\tilde{r}} + c_0\,e^{d\,\tilde{r}}, \quad \tilde{r} = \min(r,\, 800\,\mathrm{m}), \tag{3}$$

with coefficients $\{a, b, c_0, d\} = \{-6.070,\ 2.12 \times 10^{-3},\ 5.987,\ 2.25\times10^{-3}\}$. In multi-AUV operations, simultaneous uplink pings elevate the collision probability:

$$P_{\mathrm{loss}}^{\mathrm{total}}(r) = \min\big(P_{\mathrm{loss}}(r) + (N_{\mathrm{AUV}} - 1)\,P_{\mathrm{col}},\ 0.999\big), \tag{4}$$

where $P_{\mathrm{col}} = 0.05$ per additional AUV. A fix is declared lost if $u \sim \mathcal{U}(0,1)$ satisfies $u < P_{\mathrm{loss}}^{\mathrm{total}}$, or if $r > r_{\max}$. This model from [31] is applied only in the range where it is physically valid.

D. Multi-ASV Formation Geometry, Coverage and Conflict Graph

The N_{ASV} ASVs are placed at the vertices of a regular N-gon centred at the survey origin $\mathbf{0} \in \mathbb{R}^2$. The formation radius is $R_f = R_{\mathrm{HF}} + \Delta_b$, where $\Delta_b \geq 0$ is a clearance buffer. The Cartesian position of ASV_j $(j = 0, \ldots, N_{\mathrm{ASV}}-1)$ in the NED plane is:

$$\mathbf{p}_j = R_f \begin{bmatrix} \cos\left(\alpha_0 + \frac{2\pi j}{N_{\mathrm{ASV}}}\right) \\ \sin\left(\alpha_0 + \frac{2\pi j}{N_{\mathrm{ASV}}}\right) \end{bmatrix}, \quad R_f = R_{\mathrm{HF}} + \Delta_b, \tag{5}$$

with formation angle α_0 (default 0). For $N_{\mathrm{ASV}} = 1$, the formation degenerates to $\mathbf{p}_0 = \mathbf{0}$.

The maximum distance from any point in Ω to the nearest ASV is bounded by the corner-to-nearest-ASV distance:

$$d_{\mathrm{corner}} = \min_j \|\mathbf{q}_c - \mathbf{p}_j\|, \quad \mathbf{q}_c \in \left\{\pm\tfrac{L}{2}\right\}^2. \tag{6}$$

Full acoustic coverage requires $d_{\mathrm{corner}} \leq R_{\mathrm{HF}}$, giving the necessary formation radius constraint:

$$R_f \ \geq\ \frac{L}{2} - \sqrt{R_{\mathrm{HF}}^2 - \left(\frac{L}{2}\right)^2}, \tag{7}$$

valid when $R_{\mathrm{HF}} \geq L/2$. For the default parameters ($L = 60$ m, $R_{\mathrm{HF}} = 50$ m), the right-hand side of eq. (7) equals -10 m, so any positive formation radius satisfies full coverage, confirming that the two-band acoustic architecture provides adequate uplink coverage at nominal scale.

The HF uplink is a shared acoustic channel: two AUVs pinging simultaneously cause a collision if any ASV lies within range of both. Two AUVs i and j are in *acoustic conflict* if:

$$\mathrm{AC}(i,j) \ \Leftrightarrow\ \exists\, k \in [1, N_{\mathrm{ASV}}] : d(\mathbf{p}_i, \mathbf{p}_{\mathrm{ASV},k}) \leq R_{\mathrm{HF}} \ \wedge\ d(\mathbf{p}_j, \mathbf{p}_{\mathrm{ASV},k}) \leq R_{\mathrm{HF}}, \tag{8}$$

where $\mathbf{p}_{\mathrm{ASV},k}$ is the position of the k-th ASV. That means two AUVs are in acoustic conflict whenever at least one ASV can hear both of them, so simultaneous uplink transmissions could collide at that ASV. The conflict graph $G = (V, E)$ has vertex set $V = \{\mathrm{AUV}_1, \ldots, \mathrm{AUV}_{N_{\mathrm{AUV}}}\}$ and edge set $E = \{(i,j) : \mathrm{AC}(i,j)\}$. Since AUV positions change continuously, G is recomputed at the end of every downlink message.

A proper k-colouring [32] assigns colour $c(i) \in \{0, \ldots, k-1\}$ to each vertex such that adjacent vertices have different colours. AUVs sharing a colour may ping simultaneously without collision. The greedy algorithm assigns:

$$c(i) = \min\big\{c \in \mathbb{N}_0 : c \notin \{c(j) : j \in \mathcal{N}(i),\ c(j) \neq -1\}\big\}, \tag{9}$$

where $\mathcal{N}(i) = \{j : (i,j) \in E\}$. The resulting colour classes $\mathcal{G}_0, \ldots, \mathcal{G}_{k-1}$ partition V and define the TDMA ping groups. By Brooks' theorem, $k \leq \Delta(G) + 1$, where $\Delta(G)$ is the maximum vertex degree, bounding the number of slots in the worst case.

E. TDMA Acoustic Protocol

A TDMA slot must accommodate: (i) ping transmission T_{P}, (ii) worst-case one-way travel time (OWTT) $\tau_{\mathrm{OT,max}}$, and (iii) a guard time T_{G} against multipath echo arrivals. All timing constraints are expressed in units of the *acoustic crossing time*:

$$t_{\mathrm{C}} = \frac{L}{c} = \frac{L}{1500}\ [\mathrm{s}], \tag{10}$$

which scales guard intervals (idle times inserted between transmissions) with the survey size and ensures the protocol remains physically valid as L changes. The uplink slot duration for a ping group is:

$$T_{\mathrm{UL}} = \max\{T_{\mathrm{P}} + \tau_{\mathrm{OT,max}} + T_{\mathrm{G}},\ T_{\mathrm{UL,min}}\}, \tag{11}$$

where $T_{\mathrm{P}} = 10$ ms (fixed hardware), and:

$$T_{\mathrm{G}} = 0.5\,t_{\mathrm{C}}, \tag{12}$$

$$T_{\mathrm{UL,min}} = 2.5\,t_{\mathrm{C}}. \tag{13}$$

The guard factor 0.5 bounds multipath delay spread within the survey area; the minimum slot factor 2.5 provides a margin for inter-agent timing jitter. Let k_{S}^{g} denote the start tick of group g's uplink slot and $f_{\mathrm{T}} = 30\,\mathrm{Hz}$ the simulation tick rate ($\Delta t = 1/f_{\mathrm{T}}$). The earliest tick at which group $g{+}1$ may begin transmitting is:

$$k_{\mathrm{S}}^{g+1} = k_{\mathrm{S}}^{g} + \left\lceil T_{\mathrm{UL}}^{g}\, f_{\mathrm{T}} \right\rceil, \tag{14}$$

where the ceiling converts the continuous-time slot duration into an integer tick count.

After all colour groups in the current round have pinged, one ASV broadcasts on the shared MF downlink channel. The broadcast payload comprises an $N_{\mathrm{hdr}} = 8\,\mathrm{byte}$ header followed by K_{fix} individual fix records of $B_{\mathrm{fix}} = 16\,\mathrm{bytes}$ each, where K_{fix} is the number of fixes accumulated during the uplink round:

$$N_{\mathrm{bytes}} = N_{\mathrm{hdr}} + K_{\mathrm{fix}}\, B_{\mathrm{fix}}\ [\mathrm{bytes}]. \tag{15}$$

The transmission duration (with protocol overhead factor $\Lambda = 2.0$) is:

$$T_{\mathrm{tx}} = \frac{N_{\mathrm{bytes}} \cdot 8 \cdot \Lambda}{R_{\mathrm{DL}}}, \qquad R_{\mathrm{DL}} = 2000\ \mathrm{bps}. \tag{16}$$

The total MF slot duration is:

$$T_{\mathrm{DL}} = \max\left\{T_{\mathrm{tx}} + T_{\mathrm{DL,G}},\ T_{\mathrm{DL,min}}\right\}, \tag{17}$$

with,

$$T_{\mathrm{DL,G}} \quad = 1.25\, t_{\mathrm{C}}, \tag{18}$$

$$T_{\mathrm{DL,min}} \quad = 10.0\, t_{\mathrm{C}}. \tag{19}$$

The large minimum downlink slot ($\alpha_{\mathrm{DL,min}} = 10.0$) is chosen conservatively to accommodate variable acoustic propagation delay across the full MF range and to allow reliable decoding at low SNR.

A fix broadcast at tick k_{B} by ASV j reaches AUV i at:

$$k_{\mathrm{D}} = k_{\mathrm{B}} + \left\lceil \left(T_{\mathrm{tx}} + \frac{d_{ij}}{c} \right) f_{\mathrm{T}} \right\rceil, \tag{20}$$

$d_{ij} = \left\| \mathbf{p}_{\mathrm{ASV},j}^{xy} - \mathbf{p}_{\mathrm{AUV},i}^{xy} \right\|$ is the horizontal separation at broadcast time. If $d_{ij} > R_{\mathrm{MF}}$, the fix is not delivered. The end-to-end latency L_{E2E} from HF ping to fix delivery is:

$$L_{\mathrm{E2E}} = \left(k_{\mathrm{D}} - k_{\mathrm{P}}\right) \Delta T, \tag{21}$$

where k_{P} is the HF ping tick and $\Delta T = 1/f_{\mathrm{T}}$.

F. Strapdown IMU Drift Model

In the absence of acoustic fixes, each AUV i propagates its estimated 2D horizontal position via strapdown dead-reckoning corrupted by a constant velocity bias $\mathbf{b}_i \in \mathbb{R}^2$ and additive noise:

$$\hat{\mathbf{p}}_i(k{+}1) = \hat{\mathbf{p}}_i(k) + \mathbf{R}(\psi_k)\Big(\mathbf{v}_k^{\mathrm{true}}\Delta t + \mathbf{b}_i \Delta t + \boldsymbol{\eta}_k \sqrt{\Delta t}\Big), \tag{22}$$

where $\mathbf{R}(\psi) \in SO(2)$ is the yaw rotation matrix and $\boldsymbol{\eta}_k \sim \mathcal{N}(\mathbf{0}, \sigma^2 \mathbf{I})$. Note that $\mathbf{v}_k^{\mathrm{true}}$ is the ground-truth velocity provided by the HoloOcean simulator; in a real deployment this would be replaced by an accelerometer-derived velocity estimate, adding a further source of error.

The simulation parameters are $\mathbf{b} = [0.06, 0.06]^{\top}$ m/s and $\sigma = 0.027\ \mathrm{m}/\sqrt{\mathrm{s}}$. The bias-induced position error grows linearly in continuous time:

$$\|\mathbf{e}_{\mathrm{DR}}(t)\| \approx \tfrac{1}{2}\,\|\mathbf{b}_i\|\, t, \tag{23}$$

and the total RMS error envelope (bias ramp plus random walk) is:

$$\sigma_{\mathrm{DR}}(t) \approx \sqrt{\tfrac{1}{4}\,\|\mathbf{b}_i\|^2\, t^2 + \sigma^2 t}. \tag{24}$$

Depth is measured independently by a pressure sensor with Gaussian noise: $\tilde{z}(k) = z(k) + \varepsilon_z(k)$, $\varepsilon_z \sim \mathcal{N}(0, \sigma_z^2)$, $\sigma_z = 0.05$ m. The vertical state component is replaced in both the IMU and fused estimates at every tick, eliminating depth-axis drift:

$$\hat{x}_{\mathrm{IMU},z}(k) \leftarrow \tilde{z}(k), \qquad \hat{x}_{\mathrm{fused},z}(k) \leftarrow \tilde{z}(k). \tag{25}$$

Upon delivery of fix $\hat{\mathbf{z}}_{i,k}$, the horizontal position estimate is updated via a two-step predict–correct scheme with gain $\gamma \in (0, 1]$:

$$\hat{\mathbf{p}}_i^{-}(k) = \hat{\mathbf{p}}_i(k{-}1) + \mathbf{R}(\psi_k)\big(\mathbf{v}_k^{\mathrm{true}} + \mathbf{b}_i\big)\Delta t, \tag{26}$$

$$\hat{\mathbf{p}}_i(k) = \hat{\mathbf{p}}_i^{-}(k) + \gamma\big[\hat{\mathbf{z}}_{i,k} - \hat{\mathbf{p}}_i^{-}(k)\big]. \tag{27}$$

Under the EKF interpretation with measurement matrix $\mathbf{H} = \mathbf{I}$, the posterior covariance satisfies $\mathbf{P}^{+} = (1{-}\gamma)\mathbf{P}^{-}$. The fixed gain $\gamma = 0.90$ is used throughout BIND-USBL, applying 90% of the innovation as a position correction at each fix delivery. Fixes from the ASV are stored in a per-AUV min-heap priority queue keyed on delivery tick k_{D}, ensuring causal application and consistent temporal ordering even under variable acoustic delay.

III. Simulation Results

We evaluate BIND-USBL in *HoloOcean* [29] through a set of GPS-denied lawnmower coverage missions involving heterogeneous ASV–AUV teams. We begin with an ideal single-ASV baseline, then examine representative failure and recovery cases in larger survey areas, and finally report the full configuration sweep across ASV count, formation geometry, and survey scale.

A. Experimental Setup

All experiments are conducted through simulations in *HoloOcean*. AUVs execute Dubins-smooth boustrophedon lawnmower missions at a fixed depth of 10 m; the survey area $\Omega = [-L/2,\ L/2]^2$ is partitioned into equal-width horizontal strips, one per AUV. ASVs are deployed in a stationary regular-N-gon formation centred at the survey origin and held in station-keeping throughout each mission.

The two-band acoustic protocol described in Section II is active throughout. HF uplink parameters are $R_{\mathrm{HF}} = 50$ m and $R_{\mathrm{MF}} = 100$ m. These ranges are shorter than typical acoustic and USBL systems, where HF channels may reach several hundred metres and MF links extend to kilometre-scale distances; however, the 2:1 ratio between downlink and uplink

range is preserved, maintaining the architectural relationship between the two bands. The reduced absolute values allow the coverage-failure regime to be reached within the simulator's spatial constraints, making the interaction between survey scale, formation geometry, and acoustic coverage experimentally accessible at $L \leq 140$ m.

USBL fixes are generated using the noise and outage model of [31] (RTT quantisation, TDOA noise, AHRS heading error, range-dependent and team-size based packet loss). The IMU dead-reckoning bias is $\mathbf{b} = [0.06, 0.06]^\top$ m/s, step noise $\sigma = 0.027$ m/$\sqrt{\text{s}}$, and depth noise $\sigma_z = 0.05$ m. The complementary filter gain is fixed at $\gamma = 0.90$. All simulations run at 30 Hz; unless stated otherwise, results are averaged over 20 independent random seeds and all applicable formation angles.

Three survey area side lengths are tested: $L \in \{60, 100, 140\}$ m. The primary performance metrics are mean cross-track error (CTE) in metres, per-AUV HF coverage fraction (fraction of ping attempts heard by at least one ASV), cumulative fix count, and end-to-end acoustic latency. Results are structured to trace the progression from a well-conditioned baseline to a coverage-limited failure regime, and then to show how BIND-USBL's multi-ASV formation and scheduling framework resolves each failure mode.

B. Baseline Validation in a Single-ASV Coverage Mission

We first establish a reference operating point in which a single station-kept ASV supports four AUVs over a 60×60 m survey for $T = 300$ s. At this scale, the entire survey area lies within $R_{\text{HF}} = 100$ m of the origin: every AUV is audible to the ASV throughout the mission. The acoustic conditions are therefore ideal, and this experiment isolates the behaviour of the TDMA scheduler and the complementary filter without coverage-induced degradation.

Fig. 1 shows the spatial layout of the mission. The IMU-only trajectory exhibits the characteristic piecewise quadratic drift predicted by eq. (23); the fused IMU+USBL trajectory tracks the planned path closely, demonstrating that a steady supply of USBL fixes is sufficient to bound inertial drift.

Across five independent runs, the TDMA scheduler delivers an aggregate applied fix rate of 0.994 Hz (in average 298.2 fixes over 300 s), with a per-AUV rate of 0.248 Hz and a mean inter-fix interval of 4.02 s. Fix allocation is near-uniform: 24.3%, 25.9%, 24.4%, and 25.4% across AUV_0–AUV_3. End-to-end acoustic latency is 51 ms (mean) with $p_{95} = 67$ ms. With the simulation bias $\|\mathbf{b}\| \approx 0.085$ m/s and mean inter-fix interval $T_{\text{IFI}} = 4.02$ s, the maximum bias-induced drift per fix interval from eq. (23) is $\frac{1}{2} \times 0.085 \times 4.02^2 \approx 0.69$ m, consistent with the sub-metre CTE observed in practice. This baseline confirms that the TDMA protocol correctly services the fleet at the maximum achievable rate given a single shared channel, and that the complementary filter successfully bounds drift to operationally acceptable levels.

The baseline, however, relies critically on full acoustic coverage. The next experiment investigates the consequences

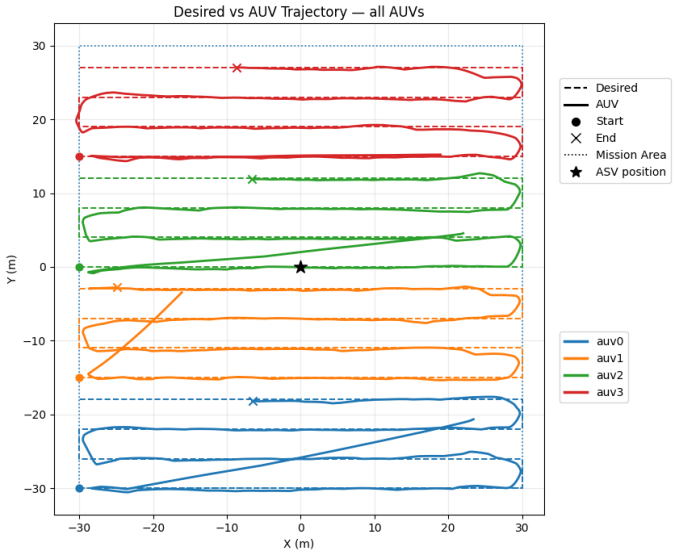

Fig. 1. Multi-AUV boustrophedon coverage at $L = 60$ m. The single ASV (star) is station-kept at the survey centroid; all four lawnmower strips fall within its HF uplink range = 100 m.

when the survey area extends beyond the single-ASV HF footprint.

C. Coverage Failure and Recovery

We scale the survey to $L = 140$ m with 3 AUVs and 1 ASV, keeping all other parameters fixed. At this scale the corner-to-ASV distance is $\|\mathbf{q}_c - \mathbf{0}\| = L\sqrt{2}/2 \approx 99$ m, nearly twice the HF range of 50 m. The single centroid-stationed ASV therefore cannot provide HF coverage to the survey extremes, and some AUVs will inevitably operate outside its acoustic footprint for extended periods.

Fig. 2 shows the trajectory overview for Single-ASV configuration ($\alpha_0 = 0°$). The per-AUV breakdown reveals extreme servicing inequality driven entirely by acoustic geometry. AUV_0, whose lawnmower strip occupies the y-extreme of the survey area, exits the ASV's HF footprint almost immediately and never re-enters it for meaningful durations. It achieves only 9% HF coverage, receiving just 19 fixes over the full 300 s mission.

The consequence is clear in Fig. 3: AUV_0's cumulative fix count flatlines early in the mission while AUV_1 and AUV_2 accumulate fixes at a near-linear rate. Deprived of corrections, AUV_0 follows the unbounded quadratic drift trajectory of eq. (23), accumulating a mean CTE of 10.0 m. AUV_1 and AUV_2, operating closer to the centroid with 70% and 58% coverage respectively, maintain CTE of 1.79 m and 2.52 m. All three AUVs travel comparable distances (182–192 m), confirming that the performance gap is entirely acoustic-geometric in origin (Table I).

This failure mode is binary, not gradual: a vehicle either remains within the ASV's HF footprint and receives adequate fixes, or it exits the footprint and drifts uncorrected. The TDMA scheduler cannot compensate for this failure mode because no valid USBL measurements are available to be

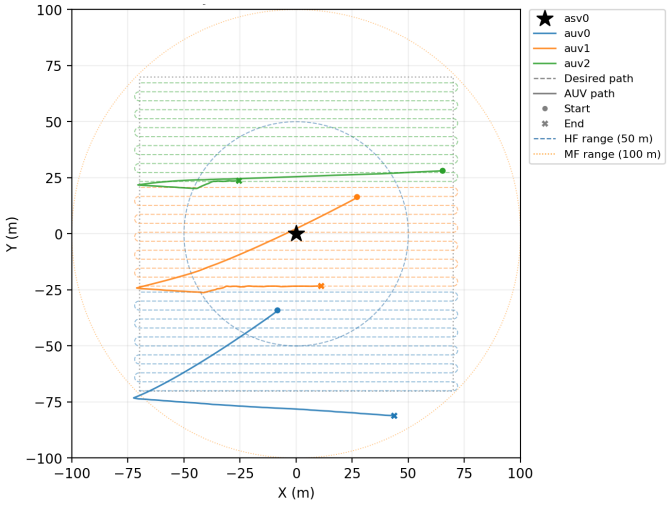

Fig. 2. Trajectory overview: $L = 140$ m, 3 AUVs, 1 ASV (star, $\alpha_0 = 0°$). The dashed blue circle marks the HF uplink range, and the dotted orange circle marks the MF downlink range. The upper lawnmower strip lies almost entirely outside the HF footprint.

TABLE I
PER-AUV METRICS FOR THE COVERAGE-FAILURE AND RECOVERY CASES ($L = 140$ M, 3 AUVS, SINGLE REPRESENTATIVE RUN).

Config	AUV	Fixes	Cov. (%)	CTE (m)	Dist. (m)
1 ASV, 0°	AUV_0	19	9	10.02	192
	AUV_1	149	70	1.79	190
	AUV_2	123	58	2.52	182
3 ASVs, 0°	AUV_0	92	79	0.56	192
	AUV_1	189	100	0.35	190
	AUV_2	185	100	0.35	182

delivered to AUV_0. The root cause is architectural: a single surface anchor with a fixed HF range cannot provide continuous coverage of a survey whose diagonal exceeds that range.

BIND-USBL addresses this failure mode directly through its N-gon formation geometry. Deploying three ASVs in an equilateral triangle formation ($\alpha_0 = 0°$) at radius $R_f = R_{\mathrm{HF}} = 50$ m distributes acoustic coverage across the survey area from multiple directions, ensuring that each lawnmower strip lies within HF range of at least one ASV at all times.

This reverses the previously observed failure mode. AUV_0, which previously received only 19 fixes with 9% coverage, now achieves 79% coverage, 92 delivered fixes, and a mean CTE of 0.56 m. AUV_1 and AUV_2 reach 100% coverage with CTE below 0.35 m (Table I). The multi-ASV deployment substantially improved coverage from 9% to 79%, demonstrating partial geometric recovery. Note that the formal guarantee of eq. (7) applies only when $R_H F \geq L/2$. The fix-rate improvement translates directly to navigation accuracy through the bounded inter-fix interval of eq. (23), demonstrating the core BIND-USBL design principle.

The coverage-failure mode is not unique to single-ASV deployments. For two ASVs, the formation angle α_0 determines whether the pair's footprints complement each other or leave symmetric gaps. Fig. 4 shows the per-AUV breakdown for two ASVs at $L = 140$ m across four formation angles.

At $\alpha_0 = 0°$, the two ASVs are aligned along the x-axis, replicating the same coverage shadow at the y-extremes. AUV_0 receives *zero* fixes and drifts to 11.1 m CTE. Rotating the formation to $\alpha_0 = 30°$ breaks the alignment symmetry: AUV_0 recovers to 55% coverage (71 fixes) and 1.37 m CTE—an $8\times$ improvement from a 30° rotation alone, with identical hardware. This confirms that for two-ASV deployments, α_0 is a first-order design variable that can determine mission success or failure. The BIND-USBL formation model provides the analytical basis for choosing α_0 to maximise the worst-case corner coverage distance.

D. Configuration Sweep: ASV Count and Survey Scale

Having established the failure mechanism and recovery pathway, we report the full parameter sweep across ASV count (up to three), formation angle (0°–90°), survey side length ($L \in \{60, 100, 140\}$ m), and AUV count (3–10). Results are averaged over 20 independent seeds and all four formation angles; the distance-normalised protocol holds total team travel approximately constant across team sizes to isolate the effect of composition from mission duration.

Fig. 5 summarises the mean CTE across the full parameter space. From these results, three design principles can be inferred. The survey scale is the dominant performance factor. At $L = 60$ m, all configurations achieve a mean CTE below 0.8 m regardless of the ASV count or team size: the survey fits within the HF footprint of a single-ASV and coverage is complete. At $L = 100$ m, single-ASV CTE grows to 1.7–3.0 m, while three ASVs hold below 0.6 m across all team sizes. At $L = 140$ m, every single-ASV configuration exceeds 4.4 m universally; three-ASV formations contain this to 0.8–1.2 m, a 4–5× reduction. This confirms the analytical coverage bound of Section II-D: once the survey corner-to-origin distance exceeds R_{HF}, a single centroid ASV cannot provide full coverage, and additional surface anchors are architecturally necessary rather than merely beneficial.

The benefit of additional ASVs is concentrated in the 1-to-3 transition. Adding a second ASV at $L = 140$ m reduces mean CTE from ∼4.8 m to ∼2.5 m. This improvement is real but angle-dependent: as the case study (Section III-C) showed, certain two-ASV angles still produce coverage shadows. The third ASV provides the critical transition to sub-1.2 m CTE by eliminating the remaining angle-dependent dead zones through triangular footprint interleaving. At $L = 100$ m, adding a third ASV reduces the CTE by a factor of 3 to 6 relative to a single ASV across all AUV counts.

The coverage fraction governs navigation quality, not the fix rate alone. As the AUV count increases from 3 to 10, the fix rate per-AUV decreases monotonically because the TDMA budget is shared between a larger fleet. This fix-rate decay does not, however, translate uniformly to CTE growth. At $L = 60$ m, CTE remains flat despite a $3\times$ fix-rate reduction because coverage is complete: all fixes that could be delivered are delivered. At $L = 140$ m with a single ASV, CTE is already saturated by coverage loss and is insensitive to further

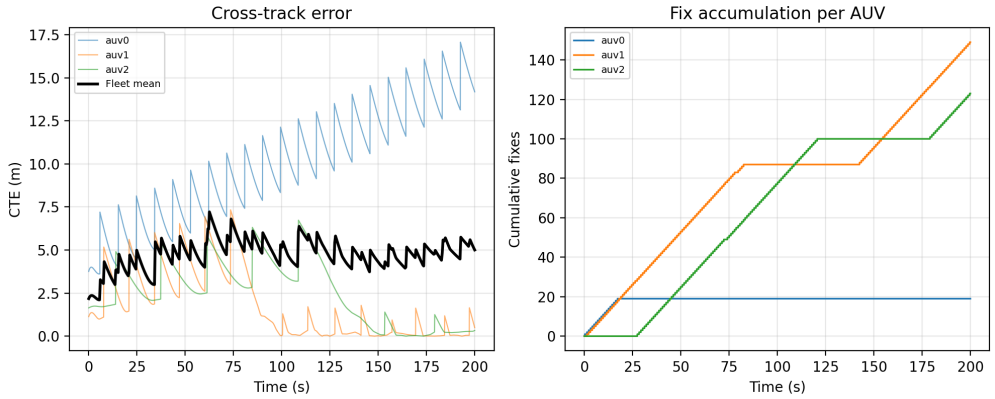

Fig. 3. Fleet metrics for the single-ASV failure case ($L = 140$ m, 3 AUVs, 1 ASV, $\alpha_0 = 0°$). Left: cross-track error over time; AUV_0 diverges unboundedly while AUV_1–AUV_2 are bounded. Right: cumulative fix count; AUV_0's count flatlines after the first few seconds, characteristic of coverage-limited starvation.

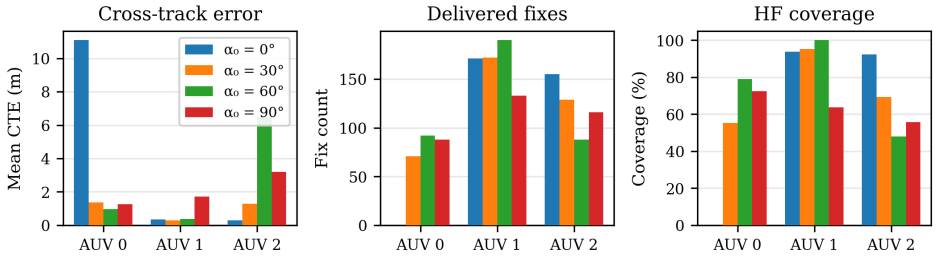

Fig. 4. Per-AUV CTE, fix count, and HF coverage for $L = 140$ m, 3 AUVs, 2 ASVs across formation angles $\alpha_0 \in \{0°, 30°, 60°, 90°\}$ (single representative run per angle). At $\alpha_0 = 0°$ the two-ASV pair is aligned along the x-axis, leaving y-extreme AUVs unserved. A 30° rotation yields an $8\times$ CTE reduction for AUV_0 with no change in hardware.

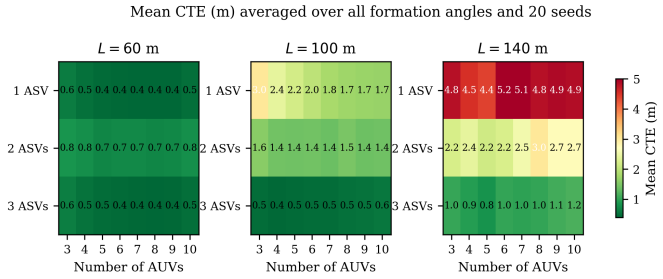

Fig. 5. Mean CTE (m) across all formation angles and 20 seeds. Columns: survey side lengths 60, 100, 140 m. Rows: ASV count; horizontal axis: AUV count. Green ≤ 1 m (well-localized); red > 4 m (navigation failure).

fix-rate changes, because the missing fixes are not a scheduling artefact but a geometric impossibility. This confirms that navigation quality is governed primarily by acoustic coverage fraction rather than fix rate, and that BIND-USBL's formation geometry is designed to address exactly this binding constraint.

Fig. 6 provides the angle-resolved breakdown, showing the mean position error and applied fix rate as a function of AUV count for each survey scale and ASV count. Three features are worth noting beyond the aggregate trends of Fig. 5. First, at $L = 60$ m (top row), all curves collapse regardless of ASV count, formation angle, or team size, confirming that the 60 m domain is coverage-saturated and performance is limited only by the TDMA servicing rate. Second, at $L = 100$ m and 140 m, the 1-ASV curves (solid lines) separate sharply from the 2- and 3-ASV curves (dashed and dotted), with the gap widening as AUV count decreases — fewer AUVs mean longer per-vehicle trajectories that extend further into the coverage-deficient extremes of the survey area. Third, the fix-rate curves (right column) are nearly identical across all ASV counts at a given AUV count, indicating that fix rate is governed by TDMA scheduling rather than formation geometry. The divergence in position error despite similar fix rates reinforces the finding that coverage fraction, not servicing rate, is the binding constraint on navigation quality at larger survey scales.

Taken together, the sweep results support the central claim of BIND-USBL and make it operationally concrete. Navigation quality in heterogeneous ASV–AUV teams is governed by the joint interaction of acoustic coverage, formation geometry, and mission scale. At $L = 60$ m, a single ASV and the TDMA scheduler suffice; at 100 m and beyond, the formation design becomes the primary performance lever. The heatmap of Fig. 5 provides a practical lookup table for mission planners: given survey dimensions and fleet composition, it specifies the minimum ASV team size needed to achieve sub-metre navigation accuracy.

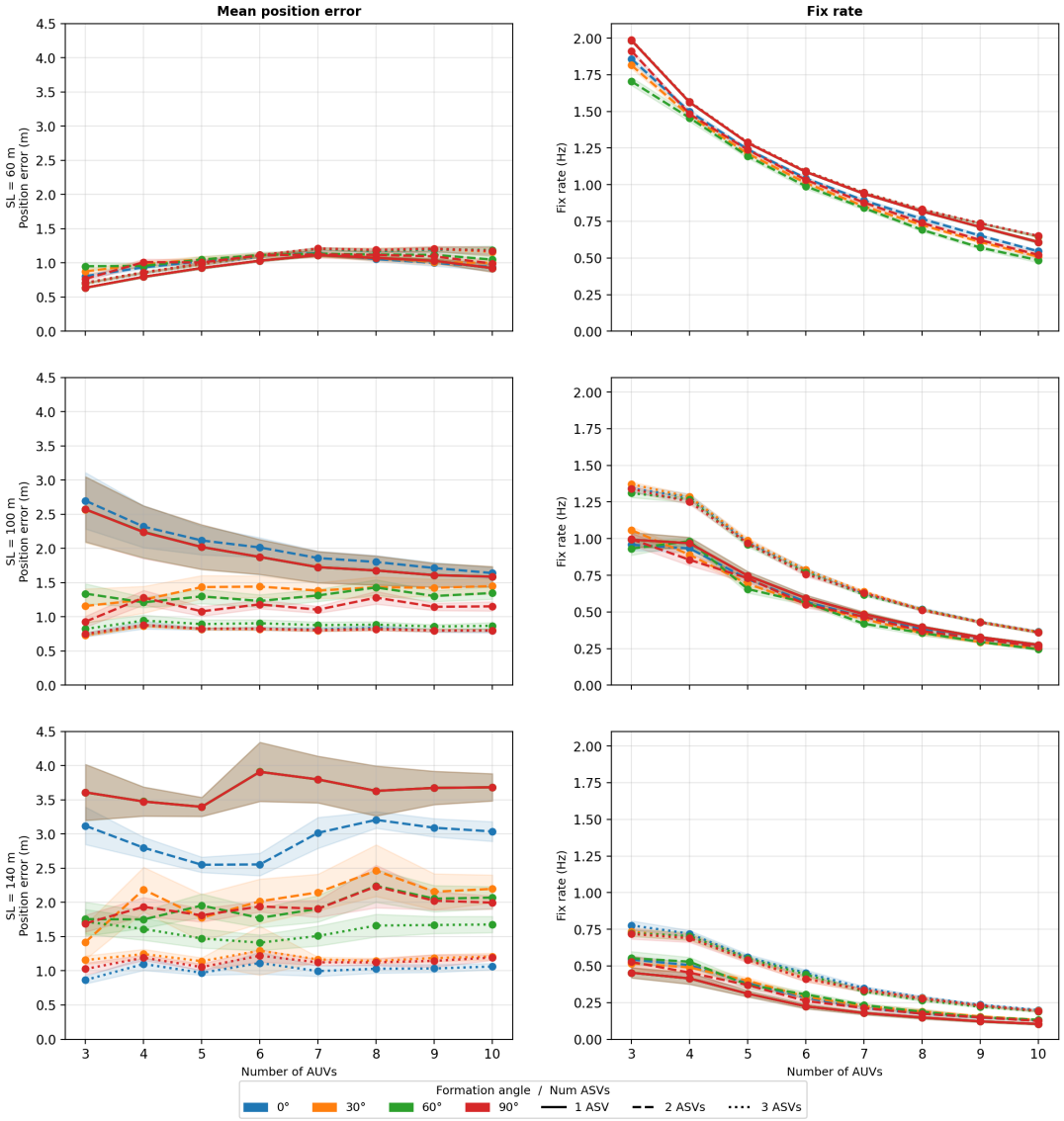

Fig. 6. Distance-normalised configuration sweep (20 seeds, mean $\pm 1\sigma$). Left column: mean position error. Right column: applied fix rate. Rows: $L = 60$, 100, 140 m. Colors denote formation angle; line styles: solid $= 1$ ASV, dashed $= 2$ ASVs, dotted $= 3$ ASVs. The sharp transition from solid to dotted lines at $L = 140$ m illustrates the binary nature of the coverage threshold.

IV. Conclusion

This paper presented BIND-USBL, a cooperative localization framework for heterogeneous ASV–AUV teams in GPS-denied underwater environments. The main result is that navigation performance is governed less by the nominal accuracy of individual USBL fixes than by their spatial and temporal availability over the mission area. A multi-ASV merged-fix scheme averages independent USBL estimates from all surface vehicles within acoustic range, reducing single-transceiver geometry sensitivity. With TDMA scheduling protocol and spatial-reuse extension based on greedy graph colouring of the AUV conflict graph. Further, a pipelined HF/MF protocol decouples uplink and downlink timing so that MF broadcasts proceed concurrently with subsequent HF uplink slots, keeping end-to-end fix latency below $0.57\,\mathrm{s}$ across all tested configurations. Simulations in HoloOcean were conducted with 3–10 AUVs and 1–3 ASVs under different formation angles and survey sizes. The results show that BIND-USBL maintains low localization error even as the mission scale increases. With three ASVs, the mean fused position error remains between 0.7–1.2 m for smaller survey areas and about 1.0–1.2 m for larger ones. In contrast, a single-ASV setup produces much higher errors, reaching about 5 m in larger survey regions. Among all tested formations for 3 ASVs, the alignment angle $\alpha_0 = 0^\circ$ gives the best performance, achieving the highest acoustic coverage and the lowest tracking error. Poorer formations, such as $\alpha_0 = 90^\circ$, significantly reduce coverage and increase localization error. As the number of AUVs increases, the localization update rate decreases because more vehicles must share the acoustic channel under TDMA scheduling.

Future work will focus on field validation, improved acoustic channel modelling, and adaptive ASV placement strategies for larger and more dynamic teams. Our results point toward principled design rules for heterogeneous marine robot teams, in which localization performance depends not only on onboard navigation but also on the deliberate design of cooperative surface support. This is especially relevant for persistent and large-area missions, where distributed surface support may become a key enabler of scalable underwater operations.

V. Acknowledgment

PK and HH acknowledge support from DFG through Germany's Excellence Strategy–EXC 2117–422037984 and the Centre for the Advanced Study of Collective Behaviour (CASCB), University of Konstanz, Germany. PK and RM acknowledge the use of ChatGPT and Claude for refining academic language and grammar; neither tool was used to generate scientific content.

References

[1] Z. Zhou, J. Liu, and J. Yu, "A survey of underwater multi-robot systems," *IEEE/CAA Journal of Automatica Sinica*, vol. 9, no. 1, pp. 1–19, 2022.

[2] R. Makam, P. Mane, S. Sundaram, and P. Sujit, "A comprehensive study on modelling and control of autonomous underwater vehicle," in *Assistive Robotics*. CRC Press, 2023, pp. 264–296.

[3] L. Paull, S. Saeedi, M. Seto, and H. Li, "Auv navigation and localization: A review," *IEEE Journal of Oceanic Engineering*, vol. 39, no. 1, pp. 131–149, 2014.

[4] M. Bresciani, G. Peralta, F. Ruscio, L. Bazzarello, A. Caiti, and R. Costanzi, "Cooperative asv/auv system exploiting active acoustic localization," in *Proceedings of the IEEE/MTS OCEANS Conference*, Sep. 2021, pp. 1–7.

[5] N. R. Rypkema, E. M. Fischell, and H. Schmidt, "One-way travel-time inverted ultra-short baseline localization for low-cost autonomous underwater vehicles," in *IEEE International Conference on Robotics and Automation (ICRA)*, 2017, pp. 4920–4926.

[6] N. R. Rypkema and H. Schmidt, "Passive inverted ultra-short baseline (piUSBL) localization: An experimental evaluation of accuracy," in *IEEE/RSJ International Conference on Intelligent Robots and Systems (IROS)*, 2019, pp. 7197–7204.

[7] N. R. Rypkema, H. Schmidt, and E. M. Fischell, "Synchronous-clock range-angle relative acoustic navigation: A unified approach to multi-AUV localization, command, control, and coordination," *Field Robotics*, vol. 2, pp. 774–806, 2022.

[8] K. Velasco, T. W. McLain, and J. G. Mangelson, "Factor-graph-based passive acoustic navigation for decentralized cooperative localization using bearing elevation depth difference," in *IEEE ICRA Workshop on Field Robotics*, 2025.

[9] J. Huang, Y. Wang, and Y. Chen, "Raspi2USBL: An open-source Raspberry Pi-based passive inverted ultra-short baseline positioning system for underwater robotics," *arXiv preprint arXiv:2511.06998*, 2025.

[10] P. Kedia, C. Apolinsky, and H. Hamann, "Developing SailSwarm: Small uncrewed sailing vessels for maritime environments," Oct. 2024, extended Abstract; presented as a poster at IROS 2024 (MHURS workshop).

[11] Z. Sun, A. Feng, J. Yu, W. Zhao, and Y. Huang, "Development of autonomous sailboat sails and future perspectives: A review," *Renewable and Sustainable Energy Reviews*, vol. 207, p. 114918, 2025. [Online]. Available: https://www.sciencedirect.com/science/article/pii/S1364032124006440

[12] Y. An, J. Yu, and J. Zhang, "Autonomous sailboat design: A review from the performance perspective," *Ocean Engineering*, vol. 238, p. 109753, 2021.

[13] T. R. Fyrvik, J. E. Bremnes, and A. J. Sørensen, "Hybrid tracking controller for an asv providing mission support for an auv," *IFAC PapersOnLine*, vol. 55, no. 31, pp. 91–97, 2022.

[14] J. E. Bremnes, T. R. Fyrvik, T. R. Krogstad, and A. J. Sørensen, "Design of a switching controller for tracking auvs with an asv," *IEEE Transactions on Control Systems Technology*, vol. 32, no. 5, pp. 1785–1800, Sep. 2024.

[15] H. Wang, S. Tong, A. Wang, W. Zhang, Z. Hu, and Z. Peng, "Heterogeneous cross domain coordinated control of asv-auv system for maritime search and rescue," *Ocean Engineering*, vol. 306, p. 117950, 2024.

[16] R. Hu, D. Wu, Z. You, D. Wu, and W. Tu, "Predefined-time terminal sliding mode cooperative trajectory tracking control for usv-auv under weak communication," *Ocean Engineering*, vol. 333, p. 121459, 2025.

[17] R. Costanzi, N. Monnini, A. Ridolfi, B. Allotta, and A. Caiti, "On field experience on underwater acoustic localization through usbl modems," in *OCEANS 2017 - Aberdeen*, 2017, pp. 1–5.

[18] Y. Liu, Y. Sun, B. Li, X. Wang, and L. Yang, "Experimental analysis of deep-sea auv based on multi-sensor integrated navigation and positioning," *Remote Sensing*, vol. 16, no. 1, p. 199, 2024.

[19] Y. Wang, S. H. Huang, Z. Wang, R. Hu, M. Feng, P. Du, W. Yang, and Y. Chen, "Design and experimental results of passive iusbl for small auv navigation," *Ocean Engineering*, vol. 248, p. 110793, 2022.

[20] H. Liu, S. Zhao, Z. Wang, J. Zhou, K. Du, and R. Shan, "An in-situ sound speed profile correction scheme for the tight-coupling integration of sins/usbl in deep-sea arv navigation," *Satellite Navigation*, vol. 6, no. 1, p. 31, 2025.

[21] J. Park and S. Cho, "Localization uncertainty estimation for autonomous underwater vehicle navigation," *Journal of Marine Science and Engineering*, vol. 11, no. 8, p. 1540, Aug. 2023.

[22] Q. Li, S. M. Naqvi, J. Neasham, and J. Chambers, "Robust cooperative navigation for auvs using the student's t distribution," in *Proceedings of the IEEE International Conference*, 2022.

[23] X. Bo, A. A. Razzaqi, X. Wang, and G. Farid, "Optimal geometric configuration of sensors for received signal strength based cooperative localization of submerged auvs," *Ocean Engineering*, vol. 214, p. 107785, 2020.

[24] M. M. Türkoğlu and E. Akyuz, "Investigation of the usv-auv cooperative environment via reinforcement learning and its impact on data collection and energy efficiency," *Ocean Engineering*, vol. 348, p. 124004, 2026.

[25] B. Das, B. Subudhi, and B. B. Pati, "Cooperative formation control of autonomous underwater vehicles: An overview," *International Journal of Automation and Computing*, vol. 13, no. 3, pp. 199–225, Jun. 2016.

[26] A. Okamoto, M. Sasano, K. Kim, and T. Fujiwara, "Development of formation control system for multiple auvs with sonar interference avoidance function," *Journal of Robotics and Mechatronics*, vol. 36, no. 2, 2024.

[27] F. Mao, D. Zhang, L. Xu, and R. Wang, "Cooperative coverage control for heterogeneous auvs based on control barrier functions and consensus theory," *Sensors*, vol. 26, no. 3, p. 822, 2026.

[28] J. Hu, L. Guo, G. Chen, Y. Chen, and J. Gao, "Cooperative target state estimation of multiple auvs based on an enhanced imm-ukf approach," *IFAC PapersOnLine*, vol. 59, no. 22, pp. 770–775, 2025.

[29] E. Potokar, S. Ashford, M. Kaess, and J. G. Mangelson, "HoloOcean: An underwater robotics simulator," in *2022 International Conference on Robotics and Automation (ICRA)*, 2022.

[30] T. I. Fossen, *Handbook of marine craft hydrodynamics and motion control*. John wiley & sons, 2011.

[31] M. Nitsch, "Navigation of a miniaturized autonomous underwater vehicle exploring waters under ice," Ph.D. dissertation, RWTH Aachen, Germany, 06 2024.

[32] R. Diestel, *Graph Theory*, 5th ed. Springer, 2017.